



## Aeroelastic Analysis of a Flapping Blow Fly Wing

Can Beker<sup>1\*</sup>, Ali Emre Turgut<sup>2</sup>, Kutluk Bilge Arıkan<sup>3</sup>, Dilek Funda Kurtulus<sup>4</sup>

<sup>1</sup> Middle East Technical University, Faculty of Aeronautics and Aerospace Engineering, [can.beker@metu.edu.tr](mailto:can.beker@metu.edu.tr)

<sup>2</sup> Middle East Technical University, Faculty of Mechanical Engineering, [aturgut@metu.edu.tr](mailto:aturgut@metu.edu.tr)

<sup>3</sup> TED University, Mechanical Engineering Faculty, [kutluk.arikan@tedu.edu.tr](mailto:kutluk.arikan@tedu.edu.tr)

<sup>4</sup> Middle East Technical University, Faculty of Aeronautics and Aerospace Engineering, [kurtulus@metu.edu.tr](mailto:kurtulus@metu.edu.tr)

### Abstract

In this study, a 3D model of the bio-inspired blowfly wing *Calliphora erythrocephala* is created and aeroelastic analysis is performed to calculate its aerodynamical characteristics by use of numerical methods. To perform the flapping motion, a sinusoidal input function is created. The scope of this study is to perform aeroelastic analysis by synchronizing computational fluid dynamics (CFD) and structural dynamic analysis models and to investigate the unsteady lift formation on the aeroelastic flapping wing for different angles of attack.

### Keywords

Micro air vehicle  
Fluid-structure interaction analysis  
Computational Fluid Dynamics  
Structural dynamic analysis  
Finite element analysis

### Time Scale of Article

Received 10 March 2020  
Revised to 14 June 2020  
Accepted 19 June 2020  
Online date 10 September 2020

### 1. Introduction

In recent times, flapping-wing micro air vehicles (FWMAVs) which are a subset of micro air vehicles have attracted great attention [1-5]. Compared to fixed-wing and rotary-wing micro air vehicles, FWMAVs are preferred since they offer great numbers of functionalities such as suitability for in-door applications, high maneuver capability, low acoustic characteristics. Lately, with the development of light-weight structures and small-scale electronic devices such as actuators, sensors, there have been proposed micro air vehicles [6].

There are two major aspects distinguish FWMAVs from other conventional MAVs which are:

- Method of producing lift and thrust forces,
- Operational flight regimes.

FWMAVs show more complex lift and thrust generating mechanisms compared to the fixed-wing micro air vehicles. Fixed-wing aircraft convert relative airstream velocity in to lift force and utilizing a mounted engine on

the wing for propelling their body. Bio-inspired flying robots generate lift and thrust force with airfoils in plunging and pitching motion. The second difference between fixed and flapping wing MAVs is the operational flight regime. Since the bio-inspired flapping systems are unable to fly fast as much as fixed-wing aircraft, they have to deal with the low Reynolds regime and produce sufficient lift and thrust force.

Even though the leading-edge vortex (LEV) associated studies dates back to the first era of aviation history, understanding the important role of the vortex structures for enhancing lift and thrust capabilities of the flapping wing systems have been attracting a great deal of attention for nearly 20 years [7]. Investigated the effect of LEV structures by performing an experimental study. The proposed study shows that LEV structures occur on the upper surface on an up-scaled blowfly wing and creates a low-pressure region. This behavior leads to the occurrence of stall delay and enhances the lift capacity of the proposed wing [8]. Investigated the blowfly wing and hawkmoth wing in different Reynolds number regimes by performing computational fluid dynamics (CFD) study and, researchers showed that the

\*: Corresponding Author Can Beker, [canbkr@gmail.com](mailto:canbkr@gmail.com), Tel: +90 312 210 2471  
DOI: [10.23890/IJAST.vm01is01.0103](https://doi.org/10.23890/IJAST.vm01is01.0103)

generated lift is directly proportional to the Reynolds number. Besides, it is shown that as the Reynolds number decreases the formation of the LEV structures changes its shape from the conical section to the cylindrical section [8].

There are numerous numerical studies that have been proposed to characterize FWMAV structures from the aerodynamical standpoint. Essentially, the performed by the researchers in this field assume the flapping wing as rigid [9]. However, making rigid-wing assumptions underestimates the aeroelastic effects that occurred on the wing. During the flapping motion, two types of motion exert on the wing structure as inertial and aerodynamic loads. Inertial loads maximize its value at the end of up-stroke and down-stroke motion since the acceleration reaches its maximum value. Aerodynamic forces relatively change depending on the velocity of the surrounds wing. The studies have been put forward in this field shows that the contribution of the inertial loads to the elastic deformation on the hawkmoth wing is more than the contribution is done by aerodynamic loads [10]. Researches performed fluid-structure interaction analysis to investigate how aeroelasticity contributes to the wing deformation [11].

Fluid-structure interaction (FSI) analyses combine the structural dynamic and fluid dynamic equations and solve both formulations simultaneously. Nakata et al. [9] report that the lift capacity of hawkmoth increases with the flexibility of the proposed wing. In the first step of the FSI, the pressure distribution is obtained for the proposed structure in the CFD domain. Then the pressure distribution is transferred to the structural dynamics domain and the imposed on the body of the corresponding structure and deformed body is obtained. Utilizing the deformed body of the structure, a dynamic analysis is solved for one increment and inertial loads are imposed on the structure. Lastly, the final position of the nodal coordinates of the deformed body is transferred to the CFD domain and, a CFD analysis is performed based on the updated elastically deformed body. The schematic view of how employing the incremental-iterative solution in fluid-structure interaction analysis is given in Figure 1.

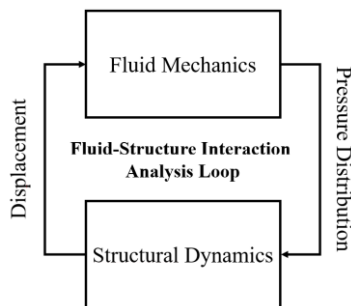


**Fig. 1.** Fluid-structure interaction analysis

In this study, how the aerodynamic characteristic of the Calliphora Erythrocephala wing varies with the angle of attack is investigated by flapping at a constant frequency.

## 2. Method

### 2.1. Wing Model

In this study, a blowfly wing designed by Konkuk University is used as a reference model [12,13]. The chord length and the half-span of the utilized wing are 29.15 mm and 58.47 mm respectively. The schematic view of the proposed wing is given in Figure 2.

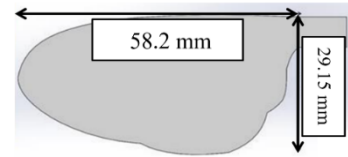


**Fig. 2.** Wing Model

The flapping angle of the proposed system is  $41.5^\circ$  and the flapping frequency is set as 11.2 Hz as given in Figure 3 [13].

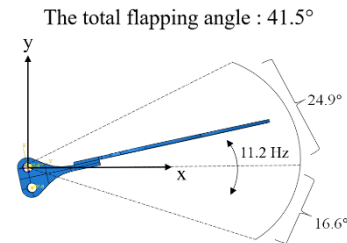


**Fig. 3.** The total flapping angle and flapping frequency

### 2.2. Fluid-Structure Interaction Model

#### Structural Dynamics Model

In the presented study, a dynamic-implicit model is defined for solving the structural-dynamics model with  $5 \times 10^{-4}$  seconds increment. The linear-elastic material properties of plexiglass material are defined to wing part in the model. Linear-elastic material properties of the plexiglass are given in Table-1.

**Table1.** Material properties of the plexi-glass

| Material    | Elastic Modulus (MPa) | Density (gr/cm <sup>3</sup> ) | Poisson's Ratio |
|-------------|-----------------------|-------------------------------|-----------------|
| Plexi-glass | 3100                  | 1.04                          | 0.35            |

The C3D8 linear-hexagonal cell grids are designated for the structural dynamics model. The total number of nodes and cells are given in Table 2.

**Table 2.** Mesh properties

| Mesh type | Number of Cell | Number of Nodes |
|-----------|----------------|-----------------|
| C3D8      | 2474           | 3816            |

A rotational periodic boundary condition is defined as sinusoidal input (Eq. 1) with 12 Hz from the pivot point of the proposed analysis model. In the Eq. 1, the  $\theta$  and  $f$  define the flapping angle and the flapping frequency as  $41.5^\circ$  and 11.2 Hz respectively. The illustration of the defined boundary conditions of the proposed structural dynamics model is given in Figure 4.

$$A = \frac{\theta}{2} \sin(2\pi ft)$$

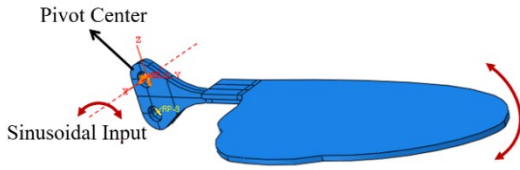


**Fig. 4.** Boundary conditions

### 2.3. Computational Fluid Dynamics Model

For the proposed study the Reynolds number is 6000. In this framework, a laminar, implicit analysis step with

$5 \times 10^{-4}$  seconds increment is defined for the CFD model. The fluid domain created for the CFD model is given in Figure 5. The proposed study is employed for hover mode. The air density is defined for the fluid domain as  $1.21 \text{ kg/m}^3$ .

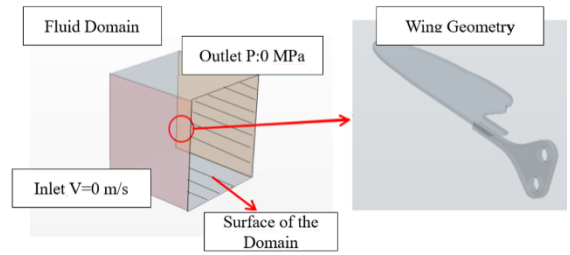
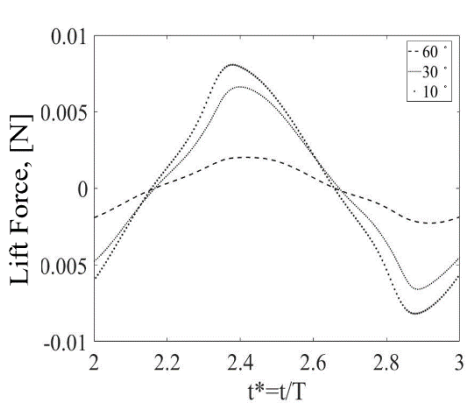


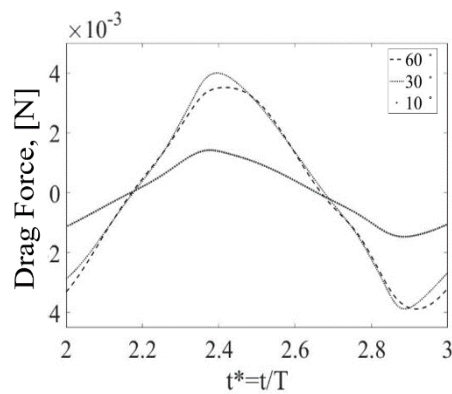
**Fig. 5.** CFD model

**Table 3.** CAD, FEA and CFD model cases for varying angle of attack

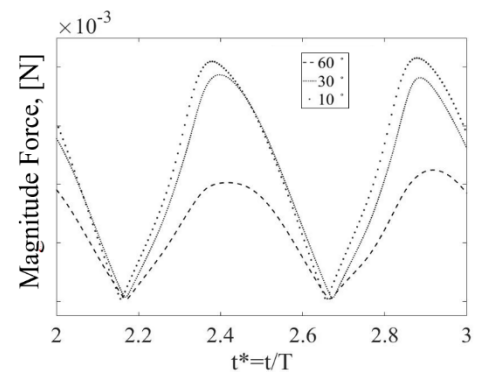
| Angle of attack | CAD Model | Structural Dynamics Model | CFD Model |
|-----------------|-----------|---------------------------|-----------|
| 10°             |           |                           |           |
| 30°             |           |                           |           |
| 60°             |           |                           |           |



(a)



(b)



(c)

**Fig. 6.** Force results (a) Lift force (b) Drag force (c) Magnitude force

**Table 4.** CAD, FEA and CFD model cases for different mean angles of attack

| Non-dimensional Time ( $t^*=t * f$ ) | Wing Position                                                                       |
|--------------------------------------|-------------------------------------------------------------------------------------|
| 2.0                                  |    |
| 2.2                                  |    |
| 2.4                                  |    |
| 2.6                                  |    |
| 2.9                                  |  |

In this study, the aerodynamic forces created by flapping motion for different mean angles of attack are investigated. Within this scope, models are created for 10°, 30° and 60° angles of attack and results are presented. The FEA models for the presented study is given in Table 3.

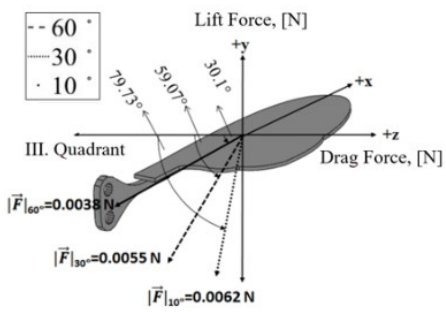
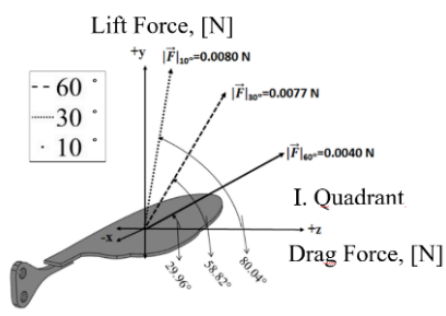
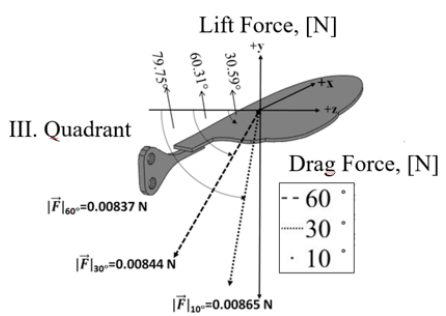
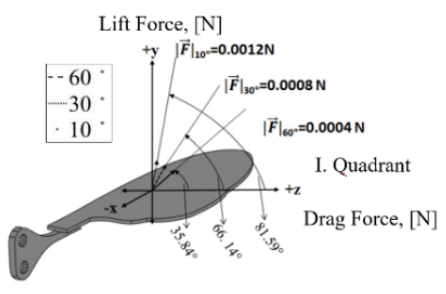
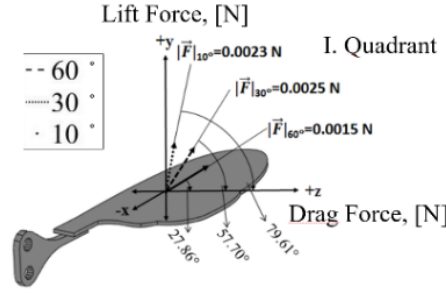
**3. Results**

The drag, lift and total forces obtained from FSI solutions for different mean angles of attack are given in Figure 6. It is observed that the resultant aerodynamic forces deviate from sinusoidal flapping motion input. The direction of the magnitude force results achieved for models with distinct angle of attacks are given in Table 5.

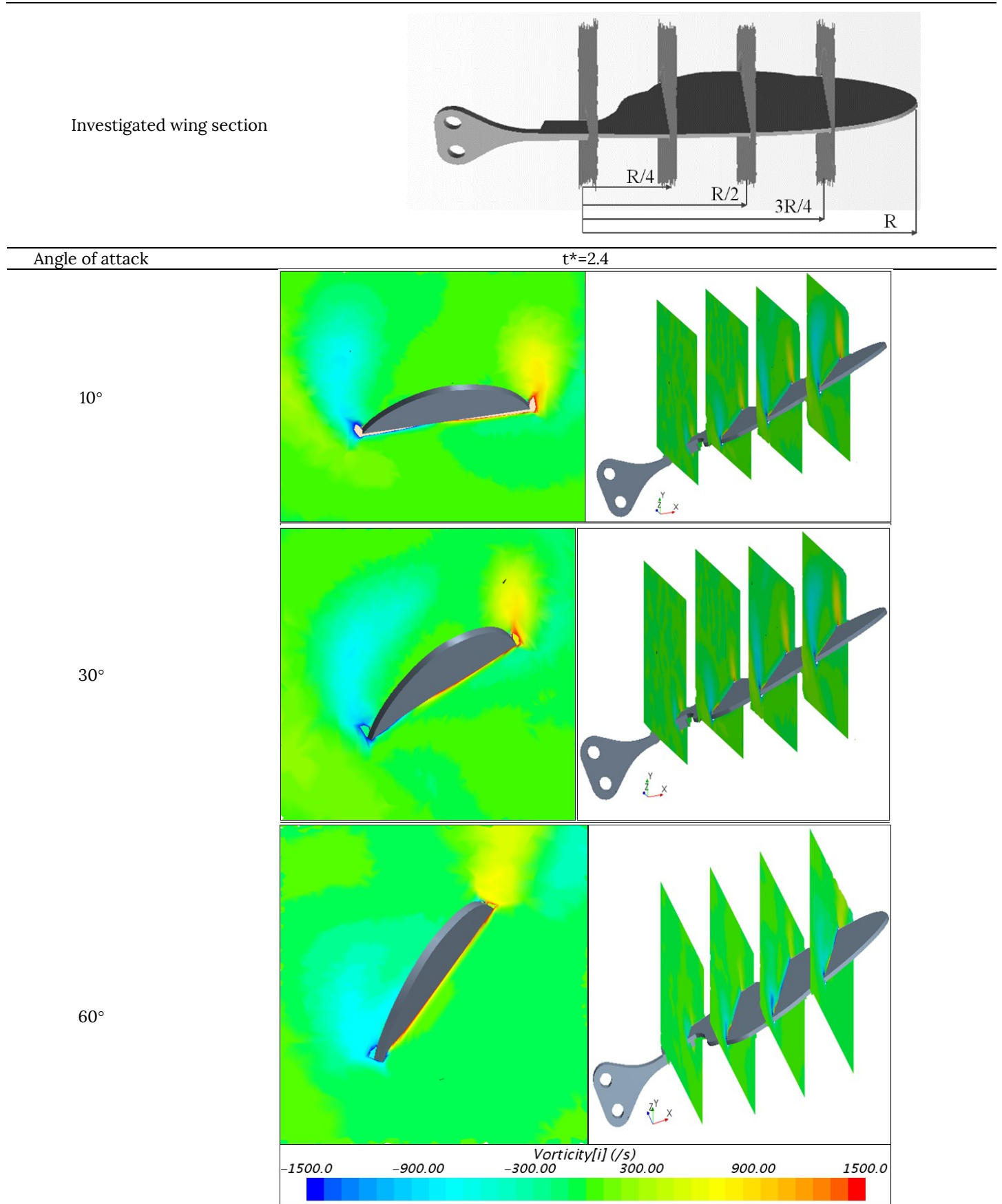
Even if the drag force for the models with 30° ve 60° angles of attack are quite similar, the difference between two models for lift force. The vortex and pressure contour results at  $t^*=2.4$  are investigated for the four different sections for the proposed wing and given in Table 6 and Table 7 respectively.

The time-dependent elastic tip deflection of the proposed wing is investigated in comparison with the rigid case. The investigated point of the proposed wing is pinpointed and given in Figure 7. The comparison of the deflections between the rigid and elastic wings are given in Figure 8.

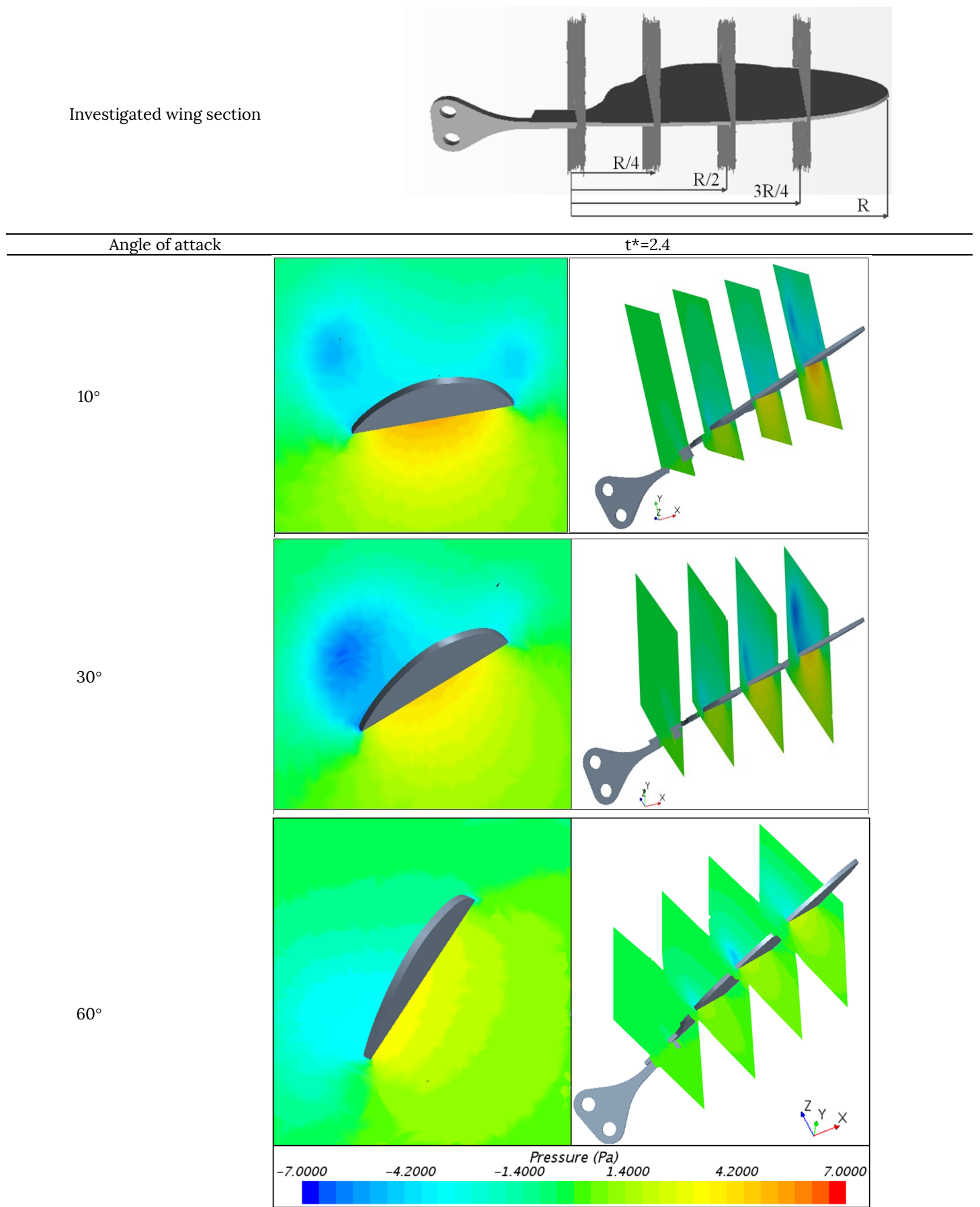
**Table 5.** Time dependent magnitude force and its direction

| Force magnitudes and directions for distinct non-dimensional times                                                                                                                                                                                                                                                                                                        |                                                                                                                                                                                                                                                                                                                                                                            |                                                                                                                                                                                                                                                                                                                                                                                  |                                                                                                                                                                                                                                                                                                                                                                           |                                                                                                                                                                                                                                                                                                                                                                            |
|---------------------------------------------------------------------------------------------------------------------------------------------------------------------------------------------------------------------------------------------------------------------------------------------------------------------------------------------------------------------------|----------------------------------------------------------------------------------------------------------------------------------------------------------------------------------------------------------------------------------------------------------------------------------------------------------------------------------------------------------------------------|----------------------------------------------------------------------------------------------------------------------------------------------------------------------------------------------------------------------------------------------------------------------------------------------------------------------------------------------------------------------------------|---------------------------------------------------------------------------------------------------------------------------------------------------------------------------------------------------------------------------------------------------------------------------------------------------------------------------------------------------------------------------|----------------------------------------------------------------------------------------------------------------------------------------------------------------------------------------------------------------------------------------------------------------------------------------------------------------------------------------------------------------------------|
| t=2.0                                                                                                                                                                                                                                                                                                                                                                     | t=2.2                                                                                                                                                                                                                                                                                                                                                                      | t=2.4                                                                                                                                                                                                                                                                                                                                                                            | t=2.6                                                                                                                                                                                                                                                                                                                                                                     | t=2.9                                                                                                                                                                                                                                                                                                                                                                      |
|  <p>Force diagrams for t=2.0 showing lift and drag forces in the III. Quadrant. Angles: 79.73°, 59.07°, 30.1°. Magnitudes: <math> \vec{F} _{60^\circ}=0.0038\text{ N}</math>, <math> \vec{F} _{30^\circ}=0.0055\text{ N}</math>, <math> \vec{F} _{10^\circ}=0.0062\text{ N}</math>.</p> |  <p>Force diagrams for t=2.2 showing lift and drag forces in the I. Quadrant. Angles: 20.96°, 58.82°, 80.04°. Magnitudes: <math> \vec{F} _{10^\circ}=0.0080\text{ N}</math>, <math> \vec{F} _{30^\circ}=0.0077\text{ N}</math>, <math> \vec{F} _{60^\circ}=0.0040\text{ N}</math>.</p> |  <p>Force diagrams for t=2.4 showing lift and drag forces in the III. Quadrant. Angles: 79.75°, 60.31°, 30.59°. Magnitudes: <math> \vec{F} _{60^\circ}=0.00837\text{ N}</math>, <math> \vec{F} _{30^\circ}=0.00844\text{ N}</math>, <math> \vec{F} _{10^\circ}=0.00865\text{ N}</math>.</p> |  <p>Force diagrams for t=2.6 showing lift and drag forces in the I. Quadrant. Angles: 35.84°, 66.14°, 81.59°. Magnitudes: <math> \vec{F} _{10^\circ}=0.0012\text{ N}</math>, <math> \vec{F} _{30^\circ}=0.0008\text{ N}</math>, <math> \vec{F} _{60^\circ}=0.0004\text{ N}</math>.</p> |  <p>Force diagrams for t=2.9 showing lift and drag forces in the I. Quadrant. Angles: 27.86°, 57.70°, 79.61°. Magnitudes: <math> \vec{F} _{10^\circ}=0.0023\text{ N}</math>, <math> \vec{F} _{30^\circ}=0.0025\text{ N}</math>, <math> \vec{F} _{60^\circ}=0.0015\text{ N}</math>.</p> |

**Table 6.** Vortex contours about x axis for different angles of attacks at  $t^*=2.4$



**Table 7.** Pressure contours for different angles of attack at  $t^*=2.4$



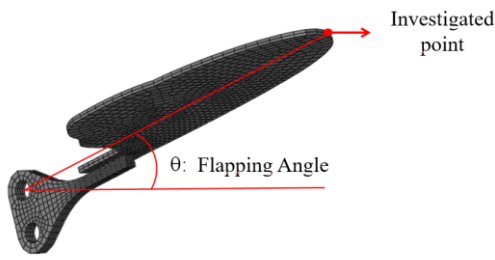


**Fig. 7.** The Investigated point

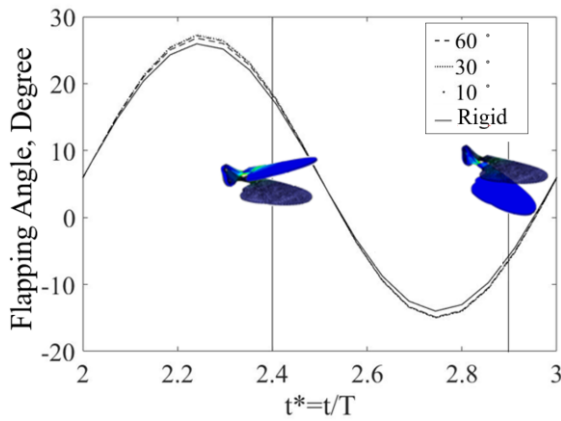


**Fig. 8.** Instantaneous aeroelastic effect to the tip deflection of the proposed wing

The time-dependent force results given in Figure 6, show that as the angle of attack increases the peak lift force value decreases concordantly. On the other hand, finding the mean force values using equation (2) gives significant evidence that the mean lift force is directly proportional to the angle of attack. In (2)  $T$ ,  $t^*$  and  $F$  refer to period, non-dimensional time and force value (lift or drag) belong to corresponding time interval respectively.

$$t^* = \frac{1}{T} \int_{t^*=2}^{t^*=3} F dt \quad (2)$$

The mean lift force results varying with the angle of attacks are given in Table 8. Negative lift force is obtained for the models with 10° and 60° angles of attack, on the flip side positive lift force is obtained for the model with 30°. Based on the given vortex results in Table 6, as the angle of attack increases the LEV (leading-edge vortex) decreases and nearly disappears at the 60° angle of attack analysis case. The time-dependent lift force results are given in Figure 6a presents that the 10° angle of attack model exhibits greater lift force amplitude compared to the analysis cases with 30° and 60° angle of attack. The minimum drag force amplitude is attained for the 10° angle of attack model. The 10° angle of attack model shows the greatest magnitude force characteristic among the

proposed flapping case models as given in Figure 6c. As it is seen from Table 6, even though the LEV structures for each model don't show a significant difference visually, the 10° angle of attack model shows greater and positive mean lift force as it is given in Table 8.

**Table 8.** Lift force statistics

| Angle of attack [°] | Maximum Lift Force [N] | Minimum Lift Force [N] | Mean Lift Force [N] |
|---------------------|------------------------|------------------------|---------------------|
| 10                  | 0.00807                | -0.00818               | -0.00004            |
| 30                  | 0.00662                | -0.00659               | 0.000091            |
| 60                  | 0.002                  | -0.00226               | -0.000042           |

Drag forces varying with different angles of attack models show negative drag force in  $-z$ -direction (Figure 6b). This situation leads to the occurrence of positive thrust caused by flapping motion (Figure 6b). Drag forces for different mean angles of attack are given in Table 9. Based on Table 9, it is seen that the net negative drag forces (thrust) are achieved for the 10° and 60° angles of attack models. Also, maximum drag forces are attained from analysis models with the 10° and 60° angles of attack.

**Table 9.** Drag force statistics

| Angle of attack [°] | Maximum Drag Force [N] | Maximum Drag Force [N] | Mean Lift Force [N] |
|---------------------|------------------------|------------------------|---------------------|
| 10                  | 0.00143                | -0.00146               | -0.000024           |
| 30                  | 0.004                  | -0.00387               | 0.000055            |
| 60                  | 0.00352                | -0.00387               | -0.000051           |

The magnitude of lift and drag forces and their quadrants are given in Table 5 (Figure 6c). The aerodynamic force magnitudes for the  $t^*= 2.2$  and  $t^*= 2.6$  appear at first quadrant, for the  $t^*= 2.0$  and  $t^*= 2.9$ , the force magnitudes take negative values and results within quadrant III.

The instantaneous wing tip displacement varying with the proposed angle of attack analysis cases is given in Figure 8. Compared to the rigid case, the 60° angle of attack model shows the least elastic angular displacement. The 10° and 30° angle of attack models exhibit the greatest and least angular displacement at the end of the up-stroke of the defined flapping motion respectively. Since the proposed system performs non-symmetric flapping motion around the  $x$ -axis (Figure 3), different inertial body forces exert on the system at the end of up and downstroke motion.

The pressure contours given in Table 7 clearly show that the analysis models with the 10° and 60° angle of attacks show homogenous high and low-pressure distribution on the upper and lower wing surfaces.

#### 4. Conclusion

In this study, the 3D model of the blowfly wing (Calliphora Wing) is modelled and analysed at different angles of attack. Instantaneous tip deflections of the modelled wing are obtained and the effects aeroelasticity are investigated on the aerodynamic forces. It is concluded that the flexibility of the wing increases the lift force amplitude compared to the rigid configuration.

#### Thanks

This study is supported by TUBITAK 116M273 project under TUBITAK 1001 program.

#### Symbols

|          |   |                      |
|----------|---|----------------------|
| $f$      | : | Frequency [Hz]       |
| $\theta$ | : | Flapping angle [°]   |
| $T$      | : | Period [s]           |
| $F$      | : | Force [N]            |
| $t$      | : | Time [s]             |
| $t^*$    | : | Non-dimensional time |

#### References

- [1] Jones, K. D., Dohring, C. M., Platzler, M. F. (1998) "Experimental and Computational Investigation of the Knoller-Betz Effect". AIAA Journal, Vol. 36, No. 7. doi: 10.2514/2.505, July 1998.
- [2] Babinsky, H., Baik, Y., Bansmer, S., Beran, P., Bernal, L., Gunaydinoglu, E., Jones, A., Kang, C.-K., Konrath R., Kurtulus, D. F., Ol, M., Paquet, J.-B., Radespiel, R., Reichert, T., Rival, D. Shyy W., Ukeiley, L., Visbal, M.R., Yuan W., (2010) "Unsteady Aerodynamics for Micro Air Vehicles" NATO Technical Report, NATO RTO-TR-AVT-149, March 2010, ISBN 978-92-837-0118-7, NATO Research and Technology Organisation
- [3] Kurtulus D.F. (2011) Introduction to micro air vehicles: concepts, design and applications, VKI LS 2011-04, Recent developments in unmanned aircraft systems (UAS, including UAV and MAV), ISBN-13 978-2-87516-017-1, April 2011, pp. 1-30.
- [4] Beker, C., Turgut, A. E., Ozcan, O., Arıkan, Kutluk. B. and Kurtulus, D. F. (2017) "Design of a Novel Foldable Flapping Wing Micro Air Vehicle". AIAC-2017-138, 9'uncu Ankara Uluslararası Havacılık-Uzay Konferansı, 20-22 Eylül 2017, Ankara.
- [5] Bektas M., Kurtulus D.F., Güler A. M. (2018) "Steady-State CFD Analysis of 3D Bio-inspired Flapping Wing Models". ISSA-2018-045, International Symposium on Sustainable Aviation 2018, 9-11 July 2018, Rome Italy, ISBN 978-605-68640-2-5, pp. 66-69
- [6] Gerdes, J., Holness, A., Perez-Rosado, A., Roberts, L., Greisinger, A., Barnett, E., Kempny, J., Lingam, D., Yeh, C., Bruck, H. A. and Gupta, Satyandra K. (2014) "Robo Raven: A Flapping-Wing Air Vehicle with Highly Compliant and Independently Controlled Wings". SOFT ROBOTICS, Volume 1, Number 4, doi: 10.1089/soro.2014.0019.
- [7] Ellington, C. P., Van den Berg, C., Willmott, A. P., and Thomas, Adrian L. R. "Leading-edge vortices in insect flight". Letters to Nature, 384(6610), 626-630. doi:10.1038/384626a0, 1996
- [8] Shyy, W., Liu, H. (2007) "Flapping Wings and Aerodynamic Lift: The Role of Leading-Edge Vortices". AIAA Journal, 45(12), 2817-2819. doi:10.2514/1.33205, December 2007.
- [9] Nakata, T., Liu, H., Bomphrey, R. J. (2015) "A CFD-informed quasi-steady model of flapping-wing aerodynamics". Journal of Fluid Mechanics, 783, 323-343. doi:10.1017/jfm.2015.537, September 2015.
- [10] Combes, S. A., Daniel, T. L. (2003) "Flexural Stiffness in Insect Wings. I. Scaling and the Influence of Wing Venation". Journal of Experimental Biology, 206, p: 2979-2987. doi:10.1242/jeb.00523, June 2003
- [11] Beker, C., Turgut, A. E., Ozcan O., Arıkan, Kutluk B. and Kurtulus, D. F., (2019) "Fluid-Structure Interaction of a Four-Bar Flapping Wing Mechanism". IX ECCOMAS Thematic Conference on Smart Structures and Materials, SMART 2019 ECCOMAS-2019, 8-11 Temmuz 2019, Paris, Fransa.
- [12] Syaifuddin, M., Park, Yoon, J. K. and Goo, Nam S. (2005) "Design and evaluation of LIPCA-actuated flapping device" Smart Structures and Materials. Vol. 5764, doi:10.1117/12.5
- [13] Senol G., Arıkan K.B., Kurtulus D.F. (2017) Experimental and Numerical Results of a Flapping Wing Four Bar Mechanism, 55th AIAA Aerospace Sciences Meeting, AIAA Scitech Forum, AIAA 2017-0498, 9-13 January 2017